Advances in Robotics Research, *Vol. 1, No. 2 (2014) 127-140*
DOI: http://dx.doi.org/10.12989/arr.2014.1.2.127

A kinect-based parking assistance system

Mauro Bellone[a], Luca Pascali[b] and Giulio Reina[*]

Department of Engineering for Innovation, Università del Salento, Via Arnesano, 73100 Lecce, Italy

(Received August 1, 2013, Revised January 23, 2014, Accepted February 1, 2013)

Abstract. This work presents an IR-based system for parking assistance and obstacle detection in the automotive field that employs the Microsoft Kinect camera for fast 3D point cloud reconstruction. In contrast to previous research that attempts to explicitly identify obstacles, the proposed system aims to detect "reachable regions" of the environment, i.e., those regions where the vehicle can drive to from its current position. A user-friendly 2D traversability grid of cells is generated and used as a visual aid for parking assistance. Given a raw 3D point cloud, first each point is mapped into individual cells, then, the elevation information is used within a graph-based algorithm to label a given cell as traversable or non-traversable. Following this rationale, positive and negative obstacles, as well as unknown regions can be implicitly detected. Additionally, no flat-world assumption is required. Experimental results, obtained from the system in typical parking scenarios, are presented showing its effectiveness for scene interpretation and detection of several types of obstacle.

Keywords: parking assistance; kinect sensor; traversability map in urban environments, intelligent vehicles; driving automation

1. Introduction

Autonomous driving for ground vehicles in general, being they mobile robots or driverless cars, requires efficient characterization of the perceived scene to ensure safe navigation and perform basic tasks including path planning, obstacle avoidance and state estimation. A large body of research exists in the robotics community related to the development of robust algorithms for scene interpretation using LIDARs (Vandapel *et al.* 2004), stereo vision (Milella *et al.* 2006), and radars (Reina *et al.* 2012). The application examples have been diverse including off-road traversability analysis for planetary exploration (Gennery 1999), and off-road terrain classification in challenging vegetated areas (Reina and Milella 2012, Bellone *et al.* 2013). The last few years have also seen a lot of research towards addressing the safety issue in the automotive field through the implementation of various methods for road detection, lane departure, cruise control, precrash alarm, and pedestrian detection. As an example, in Reisman *et al.* (2004) a real-time system was presented, applied on a commercial car, able to detect moving crowd in a video sequence. The general trend is to equip all the newest car models with advanced systems to increase the level of

[*]Corresponding author, Ph.D., E-mail: giulio.reina@unisalento.it
[a] Ph.D. student., E-mail: mauro.bellone@unisalento.it
[b] Graduate Student, E-mail: luca.pascali@studenti.unisalento.it

 ISSN: 2287-4976 (Print), 2287-4984 (Online)

safety and comfort of driver and passengers. In this context, parking assistance systems may enhance the driver's ability to survey the surrounding environment preventing collisions at low speed when the driver's attention may be distracted. Many different sensor modalities have been employed for this task. For example, ultrasonic sensors were proposed by Hatano *et al.* (2007) and Spedicato *et al.* (2013). However, ultrasonic technology is not able to perform accurate 3D reconstruction of the environment and, for this reason, many researchers have investigated the possibility to apply visual sensors (Vestri *et al.* 2005, Lovegrove *et al.* 2011). As a further example, in Lalonde *et al.* (2012) an implementation of a 3D reconstruction algorithm was presented for the detection of static obstacles from a single rear-view parking camera. The most common visual sensors used for automotive applications are cameras, stereo-cameras and depth cameras. The Microsoft Kinect camera can be counted as a fusion between cameras and depth cameras, since it includes a RGB-camera and a depth sensor. The Kinect sensor can be used for the development of parking assistance systems. For example, Choi *et al.* (2012) used depth images for detecting obstacles in parking situations. However, by using both the camera and the depth sensor, it is possible to have RGB-D images. RGB-D images are composed by a set of distance information between the sensor and each point in the space, augmented with color information. By collecting a set of distances, it is possible to create a 3D map of the environment that can be converted into the vehicle's reference frame, obtaining what is usually referred to as a "point cloud". 3D point clouds are suitable for 3D representation of any kind of environment and scene segmentation (Marton *et al.* 2008).

In this work, an IR-based parking assistance system is presented. Specifically, using the Kinect sensor for scene interpretation and 3D reconstruction, a new parking assistance system is detailed. Starting from a 3D point cloud, a 2D grid-based traversability map is obtained. The traversability map is designed to be simple and user-friendly for inexperienced drivers by a simple labeling between traversable and not traversable cells. Traversable cells are classified as "ground", whereas non-traversable cells are classified as "non-ground". Generally, non-traversable cells represent obstacles and for this reason, they are marked as non-ground. The searching algorithm uses an extension of the Breadth-First-Search (BFS) method. The BFS approach was already used in the automotive field in Chih *et al.* (2011); here, a modified version of the BFS approach is used for road analysis by a moving vehicle. The ability to differentiate between ground and non-ground portions of the scene is referred to as "ground segmentation", and it is still an open research issue (Reina and Milella 2012).

Extensive tests were performed in order to verify the effectiveness of the proposed approach. The acquired scenarios include the most common parking situations in underground parking and outdoor parking lots. During the testing stage, a specific-designed holder was manufactured in order to mount the sensor in order to mount the sensor non-invasively on a commercial car that was employed as the experimental test bed. The position and orientation of the sensor is chosen to optimize the overall field of view.

The rest of the paper is organized as follows. In Section 2, an overview of the system is presented along with the description of the algorithm to generate 3D representation of the environment. In Sections 3, the parking assistance system is exposed in details, including a thorough description of the camera calibration and the BFS algorithm. Experimental results are introduced in Section 4, in which some typical common parking scenarios are analyzed to validate the proposed approach.

2. System overview

For the testing of the system during its development, it was integrated with a commercial car that served as the experimental test bed. Fig. 1 shows the Kinect sensor mounted on the front of the vehicle using a custom-built holder. A suction pad is adopted to attach the holder to the car's hood. The holder is made of aluminum profiles to ensure lightness. Its weight is around 1.5 kg. Considering the weight of the sensor, around 1.3 kg, the two parts assembled have a weight equal to 2.8 kg that is a way less than the suction pad maximum weight capability.

The holder design and its position were chosen to provide short-range sensing, i.e. the longitudinal field of view ranges from 0.20 m to 1.80 m, starting exactly from the vehicle bumper that is a requirement for parking applications. At a distance less than 0.20 m, the risk of collision is considered too high to drive and the vehicle should stop. At a distance higher than 1.80 m from the bumper, the vehicle is supposed to have enough free space in front of it.

Fig. 1 The experimental test bed equipped with a Microsoft Kinect camera for parking assistance purposes

Fig. 2(a) shows the kinematic scheme of the Kinect holder consisting of a two-link mechanism with adjustable length of both arms. The numbers 2 and 3 denote the prismatic joints, whereas the letter c denotes the revolute joint. The number 1 denotes the base joint where the holder is linked to the vehicle. The so-designed structure has three degrees of freedom. The revolute joint is positioned on the elbow, whereas the sensor is attached to the wrist 4. Fig. 2(b) shows the position of the Kinect and its field of view expressed in the vehicle reference frame (SdR_v). One can note that, the sensor is not aligned with the vehicle bumper, yet it is positioned 0.15 m backward. In this way, the field of view of the sensor starts from the vehicle bumper. Hence, this system ensures the required short-range visibility to the driver.

The Kinect camera provides 640×480 RGB-D images at 30Hz. The sensor comprises a RGB camera and a 3D depth sensor. The RGB video camera provides 8-bit RGB images with resolution of 640×480 pixels. The sensor beam is 57×43 degrees in horizontal and vertical direction, respectively. The 3D depth sensor consists of an infrared laser emitter and a monochrome depth

camera. These two sensors provide a light coding able to acquire information about the distances between the sensor and each pixel in the image. Processing of the sensor raw data is performed using the Point Cloud Library (PCL) (Cousins and Rusu 2011). PCL presents an advanced and extensive approach to the subject of 3D perception, providing support for all the common 3D building blocks that applications require. The library contains state-of-the-art algorithms for: filtering, feature estimation, surface reconstruction, registration, model fitting and segmentation. The implemented algorithm includes a filtering stage including an outlier removal and a voxelization in order to increase the robustness of the system.

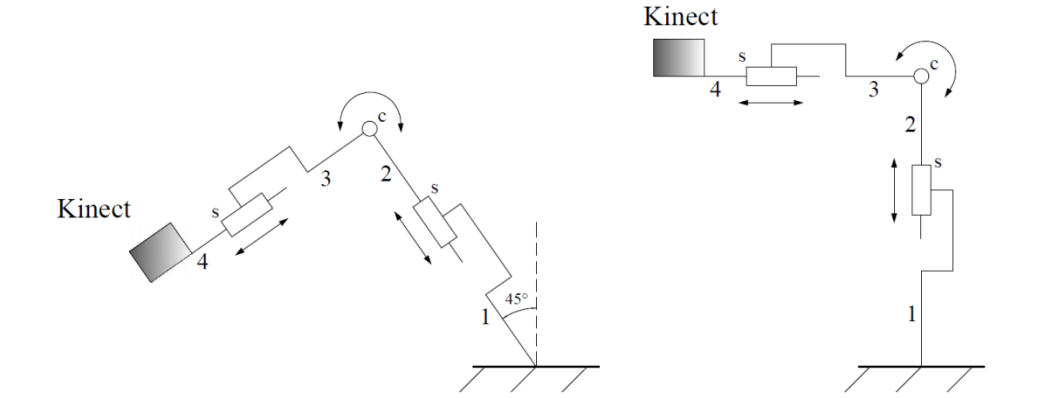

(a)

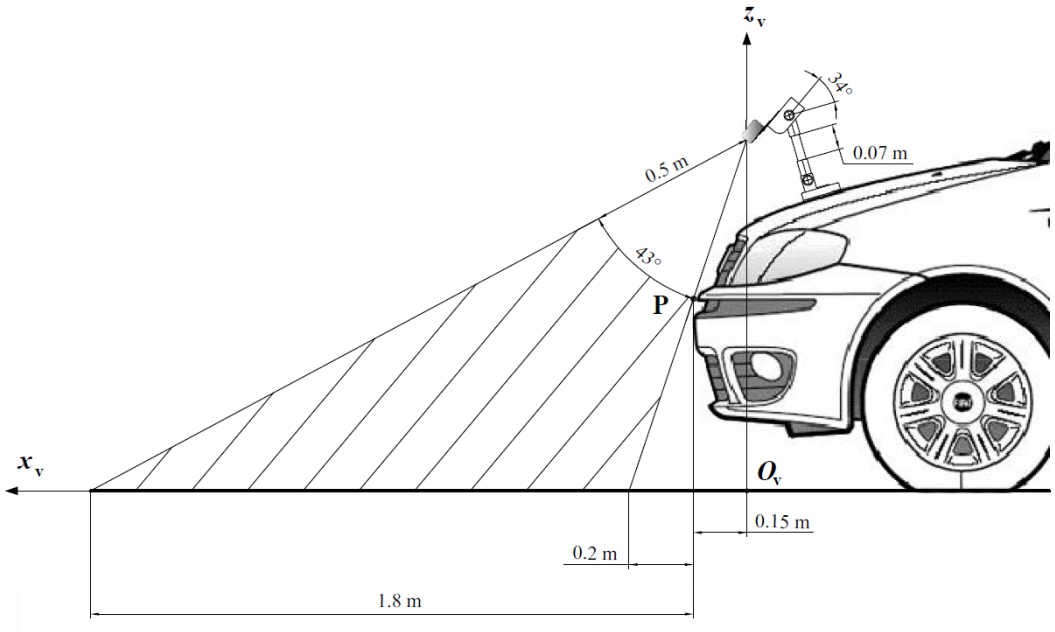

(b)

Fig. 2 (a) Kinematic scheme of the sensor holder, and (b) position of the sensor on the vehicle and longitudinal field of view

3. The parking assistance algorithm

The algorithm for parking assistance comprises the following steps: 1) camera calibration; 2) reference grid definition; 3) grid population; 4) single cell classification. The calibration step is necessary to transform the range measurements from the sensor reference frame to the vehicle reference frame. Then, the 3D point cloud is divided into a grid of 0.15 m × 0.15 m terrain patches projected onto a horizontal plane. Each 3D point is mapped to a specific cell of the reference grid. By evaluating the elevations of points in each cell is possible to assign a label to each cell. A graph-based algorithm, namely the Breadth-First-Search (BFS), is used to visit all cells of the reference grid and identify the connected cells.

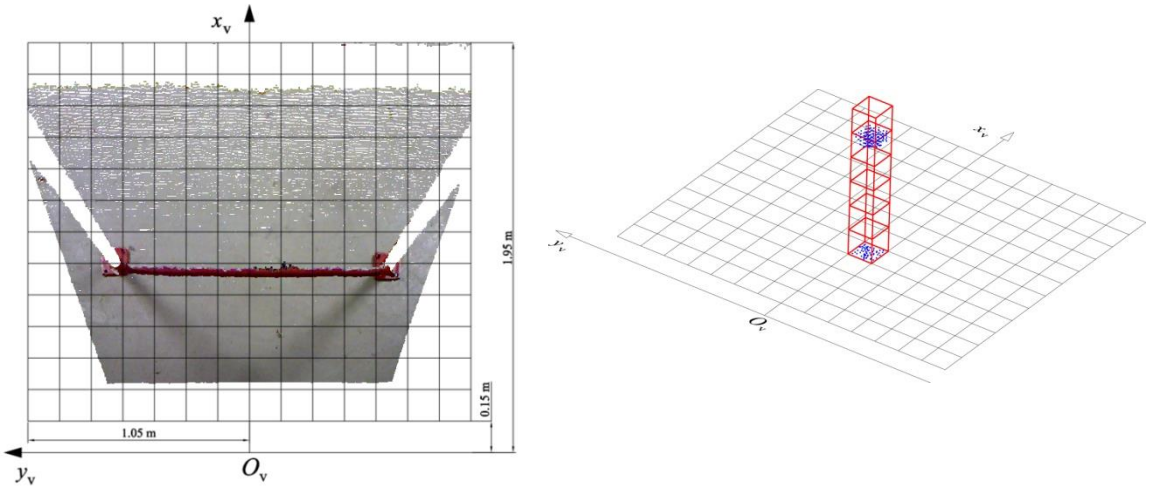

(a) (b)

Fig. 3 (a) Plan view of the reference grid in the vehicle reference frame SdR_v (O_v, x_v, y_v, z_v), and (b) elevation histogram bins for a sample cell. Blue dots: 3D points falling into the given cell

Fig. 3 helps to clarify the grid definition process showing a view of the discretized reference grid from above. Let us consider SdR_v: (O_v, x_v, y_v, z_v) as the vehicle reference frame. With reference to SdR_v, the look-ahead distance along the x_v-axis and y_v-axis results in 1.95 m and 2.10 m, respectively. Let $P = (X, Y, Z)$, be a 3D point in a Kinect scan's point cloud, where the X_v-Y_v plane is aligned with the grid and Z is the elevation of P above the grid. A cell (i, j) is assigned to each 3D point P as

$$i = \left\lceil \frac{X}{s} \right\rceil \tag{1}$$

$$j = \left\lceil \frac{Y}{s} \right\rceil \tag{2}$$

where s is the bin size, and the function $\lceil x \rceil$ gives the smallest integer greater or equal to x. In general, a cell (i, j) can have k points $P_k(i, j)$. After cells have been assigned to points, the elevation

of a cell can be computed. In detail, the histogram of the elevations (Z coordinates) of all 3D points that map to that cell is evaluated. Let a be the size of the histogram bins, then, the bin w that corresponds to elevation Z can be estimated as

$$w = \left\lceil \frac{Z}{a} \right\rceil \tag{3}$$

Fig. 3(b) shows the elevation histogram bins for a sample cell. Each point in the 3D point cloud contributes a vote to the particular bin of the histogram. In order to gain robustness to the presence of outliers, if a histogram bin shows less than m votes, it is discarded by setting the associated histogram bin value to zero. This eliminates the effect of isolated outliers. It should be noted that the elevation histogram shown in Fig. 3(b) features some 3D points on the ground and some points on an overhanging structure, i.e. the horizontal bar of the barrier. In general, if an overhanging structure detected in the scene is much higher than the vehicle, the vehicle can safely pass under it, i.e. the overhanging structure can be ignored for obstacle detection. This is the case for overpasses or road bridges. Overhanging structures can be, therefore, detected by scanning upward from the lowest non-zero histogram bin in a cell, which corresponds to the lowest surface in the given cell. If a stretch of empty histogram bins is observed that is larger than the vehicle's height, it can be disregarded (set to zero). In summary, the remaining highest non-zero bin in a cell provides the elevation of the highest point in that cell that must be considered for obstacle detection, as explained later in the paper. In the remainder of this Section, first the calibration stage is detailed. Then, the strategy for obstacle detection is described.

3.1 Camera calibration

The camera calibration stage is a delicate step, since the accuracy of the calibration determines the robustness of the parking assistance process. During the acquisition stage, the sensor provides data in the camera reference frame SdR_c (O_c, x_c, y_c, z_c). However, the driver needs information in its own reference frame and for this reason the system needs to be calibrated fin the vehicle reference frame SdR_v. In order to perform the calibration, it is necessary to locate a point in the world reference frame using a calibration grid. This camera calibration method is widely used in computer vision in order to locate the camera in a fixed reference frame (Zhang 2000, Hartly and Zisserman 2004).

In order to transform the camera reference frame into the vehicle reference frame, the following transformation matrix is required

$$T_{,\bar{c}\bar{v}} = T_{,w\dot{w}} \dot{T}_{\varsigma w} \tag{4}$$

where, $T_{c,w} \in \Re^{4\times 4}$ is the transformation matrix from the camera reference frame to the world reference frame and $T_{w,v} \in \Re^{4\times 4}$ is the transformation matrix from the world reference frame to the vehicle reference frame. Their product is $T_{c,v} \in \Re^{4\times 4}$ that is the transformation matrix from the camera reference frame to the vehicle reference frame. Specifically, $T_{c,w}$ is given by the extrinsic calibration of the camera

$$T_{c,w} = \begin{bmatrix} [r_{c,w}] & [t_{c,w}] \\ [0 \quad 0 \quad 0] & [1] \end{bmatrix} \tag{5}$$

where, $r_{c,w} \in \Re^{3\times 3}$ and $t_{c,w} \in \Re^{3\times 1}$ are the rotation matrix and the translation displacement vector of the transformation matrix $T_{c,w}$, given by

$$r_{cw} = \begin{bmatrix} l_{c_x} & l_{y} & l_{z_c} \\ m_{c_x} & m_{y} & m_{z_c} \\ n_{c_x} & n_{y} & n_{z_c} \end{bmatrix} \tag{6}$$

and

$$t_{c,w} = \begin{bmatrix} x_c^w & y_c^w & z_c^w \end{bmatrix}^{\mathrm{T}} \tag{7}$$

The scalars *l*, *m*, *n*, are the director cosines of r_{cw} along *x*, *y* and *z*-axis respectively. Similarly, the $T_{w,v}$ matrix is identified by

$$T_{wv} = \begin{bmatrix} [r_{wv}] & [t_{wv}] \\ [0\ 0\ 0] & [1] \end{bmatrix} \tag{8}$$

$$r_{wv} = \begin{bmatrix} l_{w_x} & l_{y_w} & l_{z_w} \\ m_{w_x} & m_{y_w} & m_{z_w} \\ n_{w_x} & n_{y_w} & n_{z_w} \end{bmatrix} \tag{9}$$

$$t_{wv} = \begin{bmatrix} x_w^v & y_w^v & z_w^v \end{bmatrix}^{\mathrm{T}} \tag{10}$$

Fig. 4 reports the details and nomenclature of the mentioned reference frames. The camera reference frame SdR_c has its origin O_c in the center of the camera. The world reference frame is

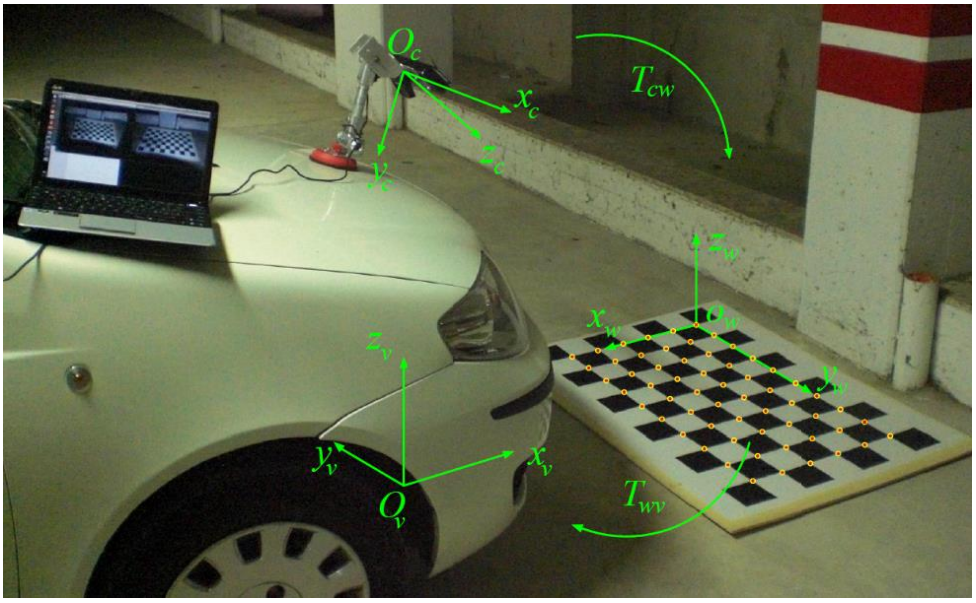

Fig. 4 Nomenclature for the Kinect Camera calibration

positioned in a known location of the space, i.e. the left-top corner of a 0.1 m square grid, called calibration pattern. The origin of the vehicle reference frame O_v is aligned with O_c along the vertical direction. Moreover, the horizontal grid plane (x_w, y_w) coincides with the horizontal vehicle plane (x_v, y_v). The calibration is performed using the MatLab calibration toolbox (Bouguet).

3.2 Classification algorithm

The goal is to classify a given cell as being traversable or not. The notion of traversability needs to be introduced defining which cells a vehicle can safely move to from its actual position. We start by defining the concept of traversability for two adjacent cells. With reference to Fig. 5, two adjacent cells c_i and c_j are traversable from each other if the maximum elevation of the two cells is similar. This can be formalized by estimating the slope $\alpha_{i,j}$ between the two cells

$$\alpha_{i,j} = \frac{z_{j,\max} - z_{i,\max}}{r} \tag{11}$$

where, $z_{i,max}$ and $z_{j,max}$ are the elevation of the cells c_i and c_j, respectively, and r is the distance between the geometric center of two adjacent cells. The two cells are defined to be traversable if $\alpha_{i,j}$ is smaller than a specific threshold α_s. Otherwise, the cells are classified as "non-traversable". The parameter α_s is a user choice and it depends on the vehicle climbing capability and on the smallest obstacle height that the system is required to detect. In our system, a value of $\alpha_s = \tan(15°)$ was found to be suitable for parking applications that corresponds to a minimum detectable height of about 8 cm.

Now, the concept of traversability can be extended to the entire grid that can be seen as a graph whose nodes are the cells of the grid and whose edges link adjacent cells that are traversable from each other. These connected cells will form the set of traversable cells T.

In the graph-theory, the BFS is a strategy for searching in a graph and it can be used to identify the connected components. Starting from a node, called the "root node", it inspects all the

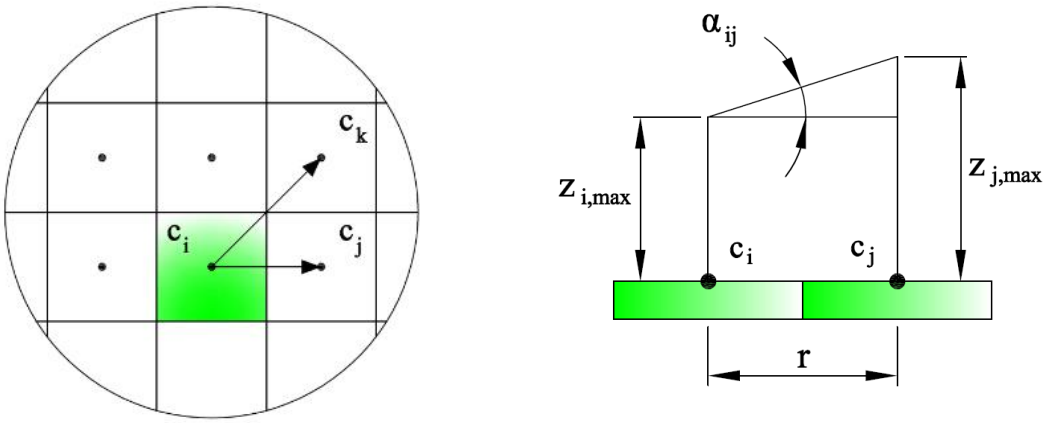

(a) (b)

Fig. 5 (a) Breadth-First-Search can be applied to identify the connected components starting form a "root" node in a graph whose nodes are the cells of the grid, and (b) geometric interpretation of the traversability condition for two adjacent cells

neighboring nodes in order to find a path to another node (Knuth and Donald 1997). In this work, an extension of the BFS is employed. Starting from the root cell, the algorithm iteratively inspects all cells, classifying them as "ground" or "non-ground".

In summary, the proposed system works according to the block diagram shown in Fig. 6.

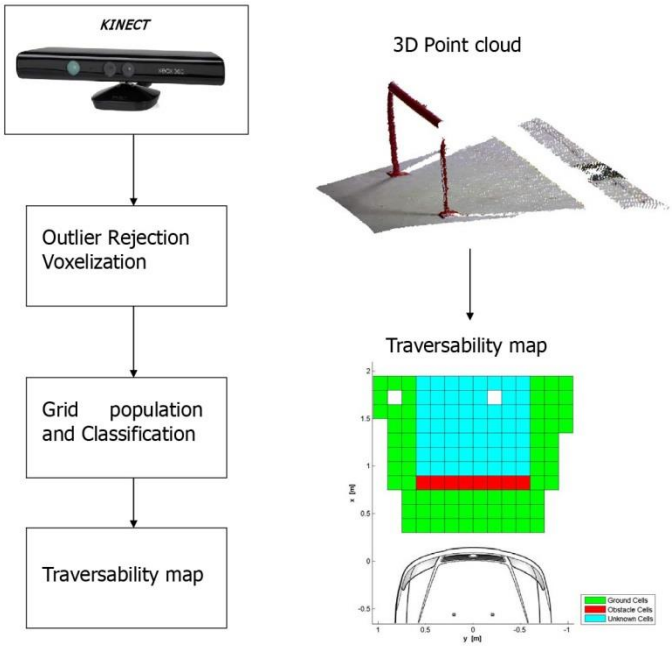

Fig. 6 Block diagram of the proposed system

4. Experimental results

Extensive tests were performed in order to verify the effectiveness of the parking assistance system in the field. A large number of scenarios and parking maneuvers were analyzed. Tests were performed in both indoor and outdoor parking. Salient results are collected in the following Figs. 7-11. In detail, Fig. 7 shows the traversability map obtained from the system for a sample image acquired as the vehicle maneuvers toward a parking spot that is delimited by a squared concrete pillar of 0.4 m×0.4 m. Cells classified as ground are marked in green, whereas red cells mark non-traversable portions of the scene. As apparent from the map, the system correctly flagged the presence of the obstacle and the drivable portion of the scene. The entire sequence comprises 60 frames acquired at a sampling rate of 1 Hz with a maximum travel speed of about 5 km/h that is typical in parking maneuvers.

The grid view was designed to ensure simplicity and readability. The original visual image is also shown on the right of the figure. Fig. 7 may represent a possible visualization layout on the dashboard of a car for the practical implementation of the system.

Fig. 8 shows a different scenario acquired during a parking maneuver in an underground parking with very low lighting condition. The duration of this acquisition is 313 seconds with a sampling frequency of 1 Hz. Since the system is based on IR-technology, it is still able to generate

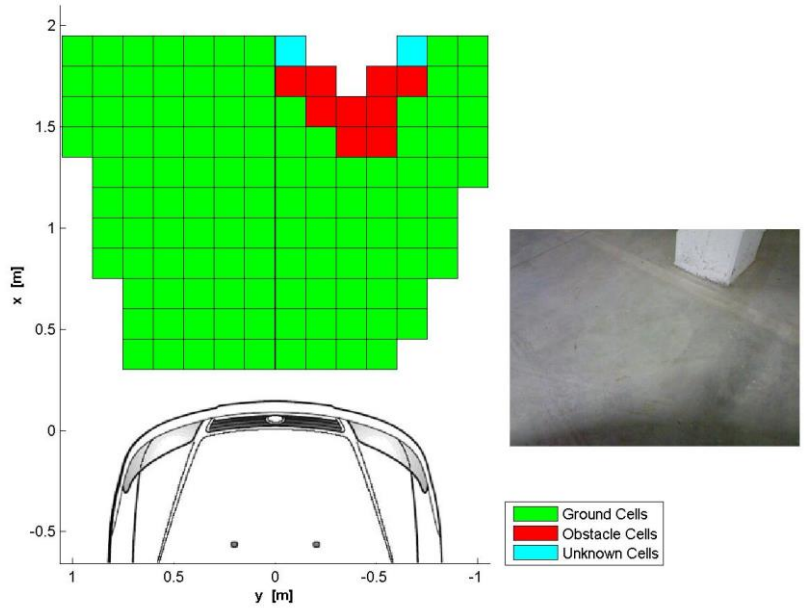

Fig. 7 Traversability map obtained from the parking assistance system at a travel speed of about 5 km/h in an underground parking where a concrete pillar was present in the scene. The original visual image is shown on the right side

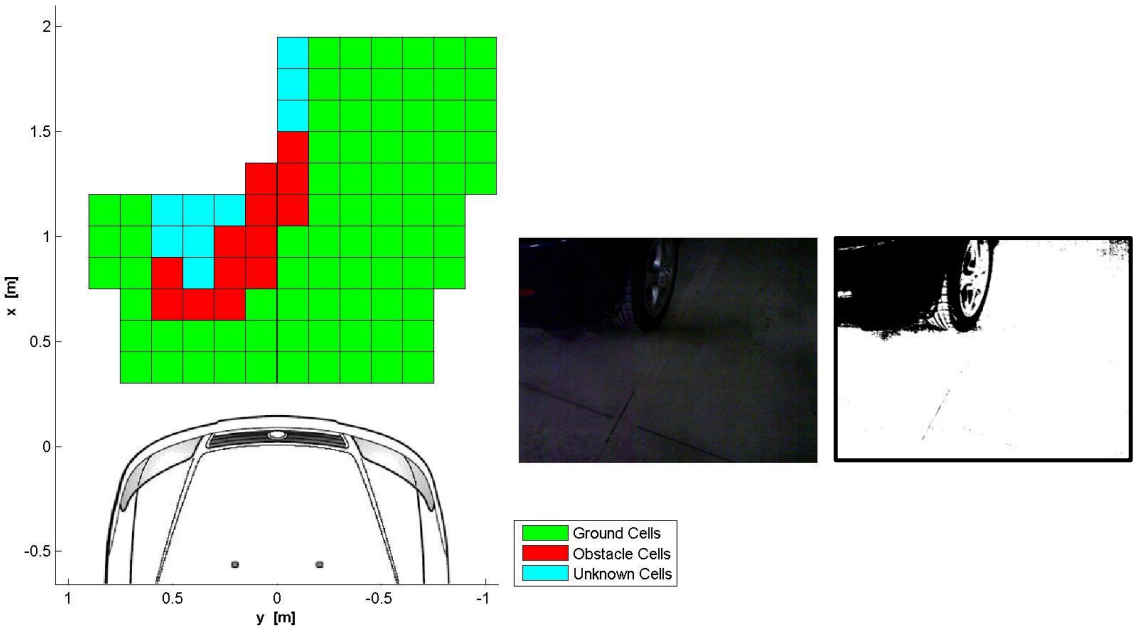

(a) (b)

Fig. 8 (a) Experimental result obtained from the system during a parking maneuvering in low-lighting condition. The traversability map is shown along with the original visual image, and (b) original image enhanced after low-light image processing

an accurate traversability map. Although the visual camera does not "see" the other car in front, as shown in Fig. 8(b) that was obtained after low-light image processing, the depth camera is able to perform range measurements allowing the algorithm to run correctly. One can note that, the grid is not completely populated and it shows some empty cells. As a matter of fact, when an obstacle is located in front on the camera, it is impossible to acquire data behind it. For this reason, some cells contain no 3D points and cannot be labeled. In addition, the grid presents cyan cells; they characterize what are referred to as the "unknown" cells. In this category fall all the cells that contain 3D data but cannot be classified by the system. This happens for cells that are directly occluded by an obstacle or cells that cannot be connected to any ground-labeled root node, i.e., that are not physically "reachable" by the car.

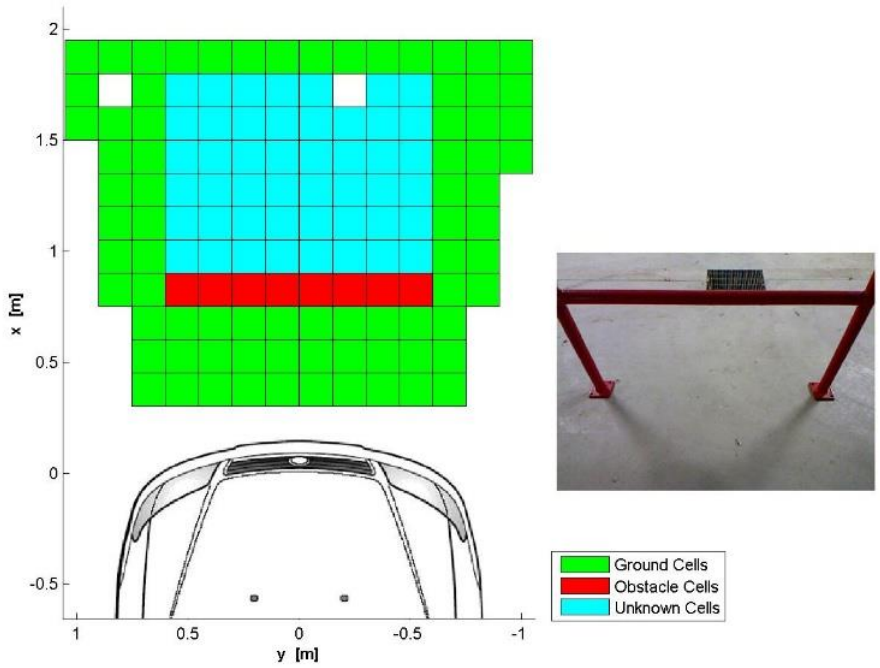

Fig. 9 Underground parking scenario showing a barrier at 0.4 m across from the vehicle. Left side and right side show the traversability map and the camera image, respectively

Another scene is shown in Fig. 9 extracted from an acquisition at 1 Hz, during a parking maneuver in the underground parking of the "Corpo Y" building at the Department of Engineering for Innovation of the University of Salento. A metallic barrier, 1.2 m wide and 1.3 m high, is located in front of the vehicle at about 0.8 m. Again, the scene is correctly interpreted by the algorithm with the horizontal bar of the barrier that is flagged as an obstacle since the overhanging structure is not higher than the car, as explained in Section 3. Note that all the cells occluded by the barrier are labeled as unknown by the system.

Fig. 10 reports a scenario acquired in an outdoor parking, instead. This scenario presents a 0.12-m diameter metallic pole, at 0.5 m in front of the car and a sidewalk behind it. Even in this case, the scene is correctly interpreted by the system. However, it should be highlight that the

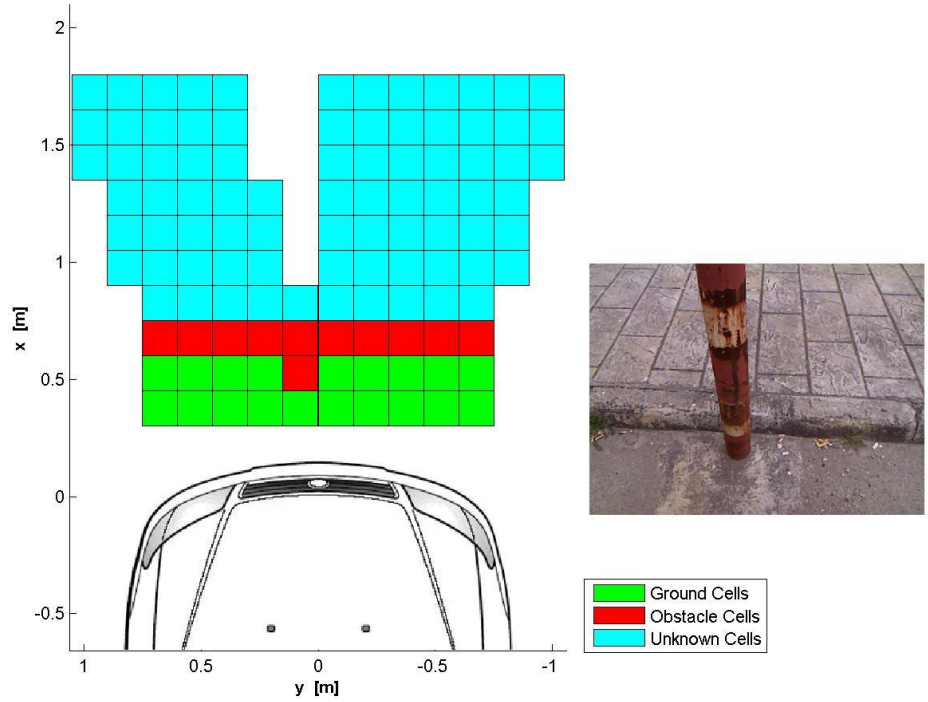

Fig. 10 Outdoor parking scenario with a metal pole at 0.5 m from the vehicle bumper and a side curb

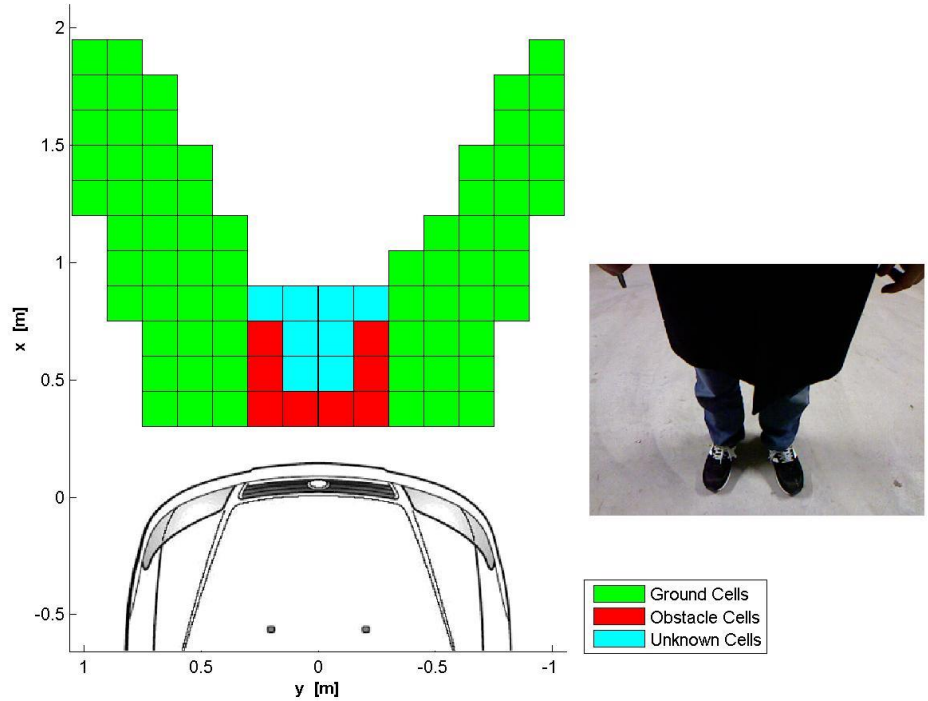

Fig. 11 Traversability map for a scene with a pedestrian across from the car

Kinect sensor has limitations in brightness, and for this reason, it cannot be applied in the case of high lighting conditions or direct sunlight. This limitation of the Kinect sensor is already known in the literature. More robust results may be achieved by the algorithm using data acquired by a high-end sensor.

Finally, the case reported in Fig. 11 includes a pedestrian at low distance (less than 0.2 m) from the vehicle bumper; also in this scene, the algorithm provides a correct traversability analysis of the scene detecting the pedestrian and the drivable areas.

In order to provide a quantitative evaluation of the system performance, the detection error of the classifier were measured for a subset of images (s_b = 80) taken from different data sets (underground and outdoor parking lot). This subset was hand-labeled to identify the ground-truth class corresponding to each cell. It resulted in an average ground detection error of 2.1% and a non-ground detection error of 6.2%.

5. Conclusions

In this paper, an IR-based parking assistance system was proposed. Throughout the paper, the scene interpretation approach has been described based on an extension of the BFS algorithm along with the 3D point cloud processing and the 2D traversability map generation. A simple and user-friendly grid view of the surrounding environment has been proposed. The simplicity of this algorithm and the grid view lend this method very well to practical application in driving assistance. During an extensive experimental campaign, the proposed parking assistance system was shown to be robust and reliable in detecting different kind of obstacles. The depth-camera used in this implementation is an off-the-shelf cost-effective camera, thus it could be easily integrated with commercial cars.

Acknowledgements

The financial support of the ERA-NET ICT-AGRI through the grant Ambient Awareness for Autonomous Agricultural Vehicles (QUAD-AV) is gratefully acknowledged.

References

Bellone, M., Reina, G., Giannoccaro, N.I. and Spedicato, L. (2013), "Unevenness point descriptor for terrain analysis in mobile robot applications", *Int. J. Adv. Robot. Syst.*, **10**, 284.

Bouguet, J. "Camera Calibration Toolbox for Matlab". http://www.vision.caltech.edu/bouguetj/calib doc/

Choi, J., Kim, D., Yoo, H. and Sohn, K. (2012), "Rear obstacle detection system based on depth from Kinect", *15th International IEEE Conference on Intelligent Transportation Systems*, Anchorage, Alaska, USA.

Cousins, S. and Rusu, R.B. (2011), "3D is here: Point Cloud Library (PCL)", *Robotics and Automation (ICRA) - IEEE International Conference on R&A*, Shanghai, China.

Gennery, D. (1999), "Traversability analysis and path planning for a planetary rover", *Auto. Robot.*, **6**, 131-146.

Hartley, R. and Zisserman, A. (2004), *Multiple View Geometry in Computer Vision*, Cambridge University Press, USA.

Hatano, H., Yamazato, T. and Katayama, M. (2007), "Automotive ultrasonic array emitter for short-range targets detection", *IEEE International Symposium on Wireless Comunication and Systems*, Trondheim, Norway.

Hsu, C.M., Lian, F.L., Ting, J.A., Liang, J.A. and Chen, B.C. (2011), "Road detection based on bread-rirst search in urban traffic scenes", *Asian Control Conference (ASCC) Kaohsiung*, Taiwan.

Donald, K.E. (1997), *The Art of Computer Programming*, Addison-Wesley, Boston.

Lalonde, J., Laganière, R. and Martel, L. (2012), "Single-view obstacle detection for smart back-up camera system", *IEEE Computer Society Conference on Computer Vision and Pattern Recognition Workshops (CVPRW)*, Ottawa, Canada.

Lovegrove, S., Davison, A.J. and Ibanez-Guzmàn, J. (2011), "Accurate visual odometry from a rear parking camera", *IEEE Intelligent Vehicles Symposium (IV) Baden-Baden*, Germany.

Marton, Z.C., Blodow, N., Dolha, M., Beetz, M. and Rusu, R.B. (2008), "Toward 3D point cloud based object maps for household environments", *Robot. Auto. Syst.*, **56**, 927-941.

Milella, A., Reina, G. and Siegwart, R. (2006), "Computer vision methods for improved mobile robot state estimation in challenging terrains", *J. Multimedia*, **1**(7), 49-61.

Reina, G., Ishigami, G., Nagatani, K. and Yoshida, K. (2010), "Odometry correction using visual slip-angle estimation for planetary exploration rovers", *Adv. Robot.*, **24**(3), 359-385.

Reina, G., Milella, A. and Underwood, J. (2012), "Self-learning classification of radar features for scene understanding", *Robot. Auto. Syst.*, **60**(11), 1377-1388.

Reina, G. and Milella, A. (2012), "Towards autonomous agriculture: automatic ground detection using trinocular stereovision", *Sensors*, **12**(9), 12405-12423.

Reisman, P., Mano, O., Avidan, S. and Shashua, A. (2004), "Crowd detection in video sequences", *IEEE Intelligent Vehicles Symposium*, Parma, Italy.

Spedicato, L., Giannoccaro, N.I., Reina, G. and Bellone, M. (2013), "Clustering and PCA for reconstructing two perpendicular planes using ultrasonic sensors", *Int. J. Adv. Robot. Syst.*, **10**, 210.

Vandapel, N., Huber, D., Kapuria, A. and Hebert, M. (2004), "Natural terrain classification using 3D ladar data", *IEEE International Conference on Robotics and Automation*, **1**, 5117-5122.

Vestri, C., Bougnoux, S., Bendahan, R., Fintzel, K., Wybo, S., Abad, F. and Kakinami, T. (2005), "Evaluation of a vision-based parking assistance system", *IEEE Conference on Intelligent Transportation Systems*, Vienna, Austria.

Zhang, Z. (2000), "A flexible new technique for camera calibration", *IEEE Tran. Pattern Anal. Mach. Intel.*, **22**(11), 1330-1334.

CC